Mechanism and Machine Theory 96 (2016) 179–191

Contents lists available at ScienceDirect

Mechanism and Machine Theory

journal homepage: www.elsevier.com/locate/mechmt

An analytical study of controlling chaotic dynamics in a spur gear system

A. Saghafi [a,*], A. Farshidianfar [b]

[a] Mechanical Engineering Department, Birjand University of Technology, Birjand, Iran
[b] Mechanical Engineering Department, Ferdowsi University of Mashhad, Mashhad, Iran

ARTICLE INFO

Article history:
Received 21 July 2014
Received in revised form 22 September 2015
Accepted 5 October 2015
Available online 11 November 2015

Keywords:
Gear vibration
Chaotic dynamics
Control

ABSTRACT

In order to design and develop an optimal gear transmission system, it is important to control the occurrence of various types of nonlinear phenomena such as bifurcation and chaotic response. This paper describes a control system for elimination of the chaotic behaviors in a gear dynamic system. Analytical approach concerning the elimination of chaos in a gear system with applying the external control excitation is given by using Melnikov method. The numerical simulations are considered to check the validity of theoretical predictions, and also to investigate the efficiency of the proposed control system to eliminate the homoclinic bifurcation and chaos in nonlinear gear systems.

1. Introduction

Gear systems are known as one of the most important sources of vibration and noise in industrial rotary machinery and power transmission systems. As a consequence, many studies have been performed for the purpose of analyzing gear dynamics. The more accurate evaluations and experimental investigations of the gear dynamic response have indicated some complicated phenomena such as regular vibrations, non-periodic or even chaotic motions on some system parameters. With the development of nonlinear dynamics theories, the nonlinear characteristics of these systems such as stability, periodic responses, bifurcations, and chaotic behaviors, have become the most interesting research areas. For instance, the experimental results, were reported by Kahraman and Blankenship [1], indicated that several nonlinear phenomena such as sub and super-harmonic resonances and chaotic behaviors occur when a spur gear pair with clearance nonlinearity subjected to combined parametric and external forced excitation is present. Also, they [2] had presented a single-degree-freedom gear system involving combined parametric excitation and clearance to analyze the steady state solutions by means of multiple term HBM approach and experimental validation. The IHBM was applied by Raghothama et al. [3] to investigate periodic responses and bifurcations of a nonlinear geared rotor-bearing system with time varying mesh stiffness and backlash. Also, the chaotic response was investigated by using numerical simulation method, and the Lyapunov exponent was calculated.

In [4], a generalized nonlinear time varying dynamic model of a hypoid gear pair with backlash nonlinearity was formulated. Computational results reveal numerous nonlinear behaviors such as sub-harmonic and chaotic responses, especially for lightly loaded and lightly damped cases. Also, Luczko [5] investigated a nonlinear model with the time varying stiffness and backlash to describe vibration of a one-stage gearbox. The possibility of existence of chaotic response was studied using numerical integration and spectrum analysis. The simulation results reveal that the system exhibits a range of quasi periodic or chaotic behaviors. In [6], Wang et al. developed a dynamic model of gear system in which sliding friction force between each tooth pair, backlash and

* Corresponding author.
E-mail address: a.i.saghafi@gmail.com (A. Saghafi).

http://dx.doi.org/10.1016/j.mechmachtheory.2015.10.002
0094-114X/

time varying mesh stiffness was considered. The complex nonlinear phenomena such as periodic response, chaos and bifurcation in system were investigated numerically.

Chang-Jian et al. [7] investigated dynamic responses of a single-degree-of freedom spur gear system with and without nonlinear suspension and found periodic and chaotic dynamics in this system. In addition, they [8] analyzed dynamics of a gear pair system supported by journal bearings. Nonlinear suspension effect, nonlinear oil film and gear mesh force are also considered. The possibility of existence of periodic, sub-harmonic and chaotic responses for some regions of the parameters were studied using numerical integration.

From the above mentioned references, one finds that non-periodic or chaotic motions have been widely found in nonlinear gear systems. Chaotic motion as unusual and unpredictable behavior has been considered as an undesirable phenomenon in vibrations of a gear system. Though the previous studies investigated the existence of bifurcation and chaos in gear dynamics, there is no attention to control these phenomena. Therefore, in order to design and develop an optimal gear transmission system, it is important to control or eliminate these phenomena.

Chaotic behavior is a very interesting nonlinear phenomenon, and it has been found in a large number of nonlinear science and engineering systems. In general, chaos is an unwanted behavior and as a consequence a major attention has received in recent years, to control and/or eliminate the chaos in these systems. Design and proper choice of system parameters are the basic ideas for suppression or elimination of the chaotic behavior. It is clear that for each parameter, there are some boundaries and limits. Beyond this area is causing serious influence on the system performance and the design is not possible. In such conditions the methods of controlling chaos are proposed. Generally, these methods have been classified in two main groups. First of them is to stabilize a determined unstable periodic orbit which is embedded in a chaotic attractor, usually achieved by the use of feedback control method [9–14]. Second is to eliminate the chaotic behaviors by applying an additional periodic excitation force or by perturbing a system parameter with small harmonic identified as non-feedback control method [15–21]. To control a determined unstable periodic orbit by feedback control methods, the OGY control approach being the most representative was introduced by Ott, Grebogi and Yorke [22]. This method does not require the information of the system equations, but one must determine the unstable periodic orbits and require performing several calculations to create the control signal. The feedback control methods seem to be efficient but have some difficulties in practical experiments.

In such cases, non-feedback control methods might be more useful and can be easily realized in practical experiments. There are numerous experimental and numerical examples of converting chaos to a periodic motion by applying an additional excitation force or by perturbing a system parameter. This method requires information of the system equations to create control forces. It does not require continuous tracking of the system state, and also, it is more robust to noise.

The main objective of this study is to develop a practical model of gear system for controlling and suppressing the chaotic behavior. To this end, a nonlinear dynamic model of a spur gear pair with backlash and static transmission error often investigated in the literature [23–25], is formulated. Non-feedback control method is used to control chaos by applying an additional excitation torque to the driver gear. The parameter space regions of the control excitation where homoclinic chaos can be eliminated are obtained analytically by generalization of Melnikov approach, which is one of the few analytical methods to study the occurrence of homoclinic bifurcation and transition to chaotic behavior in the nonlinear systems [25–33].

The organization of the paper is as follows. In Section 2, a nonlinear dynamic model of a spur gear pair including the backlash and static transmission error is formulated. The analyzing of the unperturbed system and the conditions for existence of chaotic behavior in terms of homoclinic bifurcation by using Melnikov analysis are performed in Section 3. In Section 4, the control model is described. The parameter space regions of the control excitation for elimination of chaos are investigated. In Section 5, numerical simulation results are performed to verify the theoretical analysis and show effectiveness of the proposed control system. Finally, the conclusions are presented in Section 6.

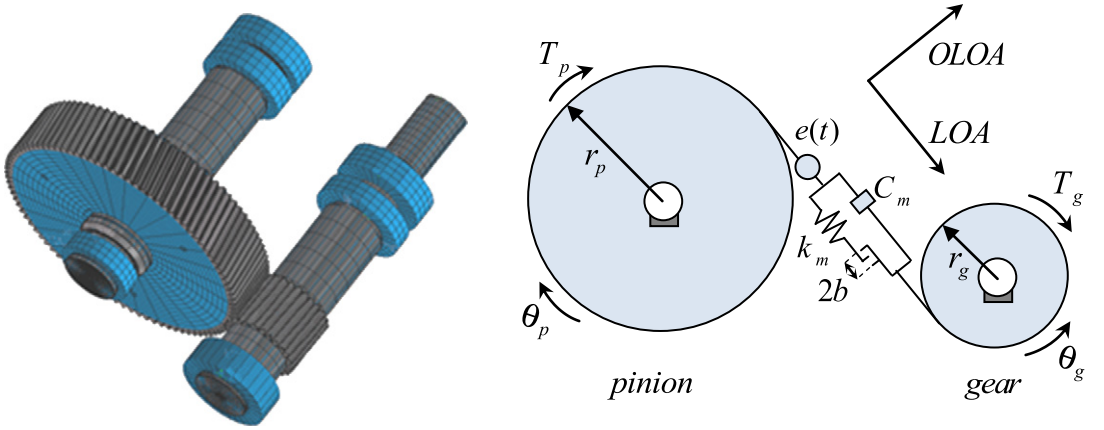

Fig. 1. Schematic of the gear model.

2. Model description and equation of motion

In this paper, a nonlinear dynamic model of a gear pair system supported by rigid mounts including the backlash and static transmission error is investigated. In this model, the gear mesh is represented as a pair of rigid disk connected by a spring damper set along the line of action, as shown in Fig. 1. The backlash function f_h, is usually used to represent gear clearances, and the displacement function $e(t)$, is also applied at the gear mesh interface to represent static transmission error. Considering θ_p and θ_g as the torsional displacements of pinion and gear, the equations of torsional motion of the 2-degree of-freedom model are given as

$$I_p\frac{d^2\theta_p}{dt^2}+r_pc_m\left(r_p\frac{d\theta_p}{dt}-r_g\frac{d\theta_g}{dt}-\frac{de(t)}{dt}\right)+r_pk_mf_h\left(r_p\theta_p-r_g\theta_g-e(t)\right)=T_p \tag{1-a}$$

$$I_g\frac{d^2\theta_g}{dt^2}-r_gc_m\left(r_p\frac{d\theta_p}{dt}-r_g\frac{d\theta_g}{dt}-\frac{de(t)}{dt}\right)-r_gk_mf_h\left(r_p\theta_p-r_g\theta_g-e(t)\right)=-T_g\,. \tag{1-b}$$

In these equations, r_p and r_g, are the base circle radius of the pinion and the gear. I_p and I_g are the mass moment of inertia of the gears. k_m and c_m represent the gear mesh stiffness and damping coefficients. Additionally, external torques T_p and T_g act on the pinion and the gear, respectively. Eqs. (1-a) and (1-b) can be reduced into Eq. (2) by defining a new variable $\tilde{x}=r_p\theta_p-r_g\theta_g-e(t)$, which is the difference between the dynamic and static transmission error.

$$m\frac{d^2\tilde{x}}{dt^2}+c_m\frac{d\tilde{x}}{dt}+k_mf_h(\tilde{x})=\hat{F}_m+\hat{F}_e(t) \tag{2}$$

Where

$$m=\frac{I_pI_g}{I_gr_p^2+I_pr_g^2}\,,\quad \hat{F}_m=m\left(\frac{T_pr_p}{I_p}+\frac{T_gr_g}{I_g}\right),\quad \hat{F}_e(t)=-m\frac{d^2e(t)}{dt^2}\,.$$

Here, m is the equivalent mass representing the total inertia of the gear pair, $\hat{F}_m$ is the average force transmitted through the gear pair, and the internal excitation term $\hat{F}_e(t)$ arises from the static transmission error. The gear pair has a clearance equal to $2b$ along the line of action, which may be designed for better lubrication and reduction of interference, or caused by wear and mounting errors. The backlash function f_h, is a nonlinear displacement function and can be expressed as

$$f_h(\tilde{x})=\begin{cases}\tilde{x}-(1-\alpha)b & b<\tilde{x}\\ \alpha\tilde{x} & -b\le\tilde{x}\le b\\ \tilde{x}+(1-\alpha)b & b<-\tilde{x}\end{cases}\,. \tag{3}$$

The static transmission error due to any manufacturing errors and teeth deformations from perfect involute form is one of the most important sources of vibration and noise in gear systems which also affect all gearbox elements. Since the mean angular velocities of the gears are constant, the static transmission error can be approximated as a periodic function, its fundamental frequency is the meshing frequency [23]. So, the static transmission error is considered as harmonic with $e(t)=e(t+2\pi/\omega_e)=e\cos(\omega_et+\phi_e)$. A non-dimensional form of the above equation can be obtained by defining

$$x=\tilde{x}/b,\ \ \omega_n=\sqrt{k_m/m},\ \ \tau=\omega_nt,\ \ \Omega_e=\omega_e/\omega_n\ ,$$
$$\tilde{\mu}=c/2m\omega_n,\ \ \tilde{F}_m=\hat{F}_m/bk_m,\ \ \tilde{F}_e=e/b\ .$$

So, the dimensionless equation of the gear pair can be written as

$$\frac{d^2x}{d\tau^2}+2\tilde{\mu}\frac{dx}{d\tau}+f_h(x)=\tilde{F}_m+\tilde{F}_e\Omega_e^2\cos(\Omega_e\tau+\phi_e) \tag{4}$$

where

$$f_h(x)=\begin{cases}x-(1-\alpha) & 1<x\\ \alpha x & -1\le x\le 1\\ x+(1-\alpha) & 1<-x\end{cases}\,.$$

f_h is a stepwise linear function and a 3-order approximation polynomial is recommended to express this function. For $\alpha = 0$, the approximated function can be expressed as: $f_h(x) = -0.1667x + 0.1667x^3$. Substituting f_h into Eq. (4), the equation of motion can be obtained as

$$\frac{d^2x}{d\tau^2} + 2\tilde{\mu}\frac{dx}{d\tau} + \left(-0.1667x + 0.1667x^3\right) = \tilde{F}_m + \tilde{F}_e\Omega_e^2\cos(\Omega_e\tau + \phi_e) \quad . \tag{5}$$

Eq. (5) presents a generalized dynamic model of a spur gear pair system. The proposed study is focused on the prediction and control of the homoclinic bifurcation and chaos in this equation.

3. Global bifurcation and chaos prediction for gear model equation

Global homoclinic bifurcation is the occurrence of transverse intersection of the stable and unstable manifolds of the homoclinic orbits and defined as a criterion for prediction of the chaotic behavior. The Melnikov analysis is one of the few analytical methods to study the global bifurcation of the system and provides the estimate in the parameter space for existence of the chaos in nonlinear systems [28–33]. In this section, the conditions for existence of the chaotic behavior in terms of homoclinic bifurcation are performed by using Melnikov analysis. In order to apply this technique and carry out this study, the homoclinic orbits, stable and unstable manifolds of the unperturbed system are derived. The damping term, the average force, and also the excitation term are considered as small perturbations to the Hamiltonian system. Thus, considering ε as a small parameter and scaling $\tilde{\mu} = \varepsilon\mu$, $\tilde{F}_m = \varepsilon f_m$, and $\tilde{F}_e = \varepsilon f_e$, the perturbed Eq. (5) can be rewritten as

$$\begin{aligned} \dot{x} &= y \\ \dot{y} &= -2\varepsilon\mu\,\dot{x} + \left(0.1667x - 0.1667x^3\right) + \varepsilon(f_m + f_e\Omega_e^2\cos(\Omega_e\tau + \phi_e)) \quad . \end{aligned} \tag{6}$$

For the unperturbed system, when $\varepsilon = 0$, the differential Eq. (6) is simplified to

$$\begin{aligned} \dot{x} &= y \\ \dot{y} &= \left(0.1667x - 0.1667x^3\right) = \left(ax - cx^3\right) \quad . \end{aligned} \tag{7}$$

The unperturbed system Eq. (7) is a planar Hamiltonian system with a Hamiltonian function as $H(x, y) = 0.5y^2 - 0.5ax^2 + 0.25cx^4$. The unperturbed system has three fixed points. From the linear stability analysis, $(+\sqrt{a/c}, 0)$ and $(-\sqrt{a/c}, 0)$ are centers, and (0, 0) is a saddle point. The saddle point is connected to itself by two homoclinic orbits, and can be obtained as

$$(x_h(\overline{\tau}), y_h(\overline{\tau})) = \left(\pm\sqrt{\frac{2a}{c}}\mathrm{sech}(\sqrt{a}(\overline{\tau})),\ \mp\sqrt{\frac{2}{c}}a\ \times\ \mathrm{sech}(\sqrt{a}(\overline{\tau}))\tanh(\sqrt{a}(\overline{\tau}))\right) \tag{8}$$

where $\tau - \tau_0 = \overline{\tau}$. Stable and unstable manifolds of the homoclinic orbits for the unperturbed system are shown in Fig. 2.

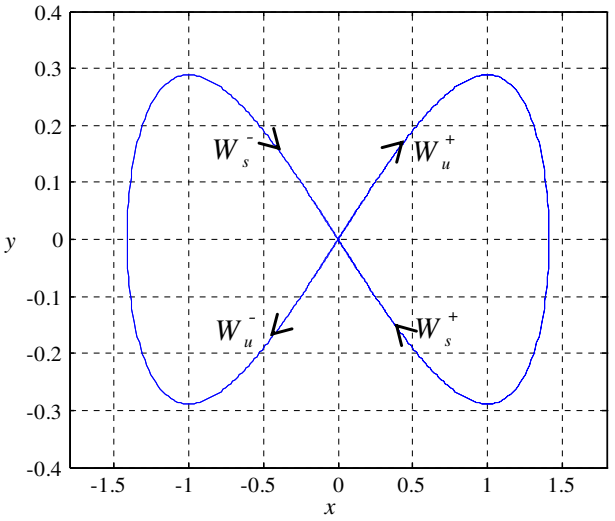

Fig. 2. Stable and unstable manifolds of the homoclinic orbits.

When the perturbation terms are added to the unperturbed system, the closed homoclinic orbits break, and may intersect manifolds. The Melnikov method measures the distance between the stable and unstable manifolds of the perturbed system in the Poincare section, and provides the estimate for transverse intersection of the stable and unstable manifolds of the homoclinic orbits, and hence the occurrence of homoclinic bifurcation and transition to chaotic behavior. According to this theory, the conditions for transverse intersection of the stable and unstable manifolds are given by $M(\tau_0) = 0$ and $dM(\tau_0)/d\tau_0 \neq 0$, where $M(\tau_0)$ is the Melnikov function and defined as follows [26,27]

$$M(\tau_0) = \int_{-\infty}^{+\infty} p(X_h(\tau-\tau_0)) \wedge q(X_h(\tau-\tau_0),\tau)d\tau = \int_{-\infty}^{+\infty} p(X_h(\tau)) \wedge q(X_h(\tau),\tau+\tau_0)\,d\tau \ . \tag{9}$$

In this equation, $X_h = (x_h, y_h)$ is homoclinic orbit. p and q represent the vector field and the perturbed vector of Eq. (6) given by

$$\begin{aligned} p(x,y) &= \left(y, ax-cx^3\right) \\ q(x,y,\tau) &= (0, -2\mu\,\dot{x} + f_m + \ \Omega_e^2 f_e \cos(\Omega_e\tau+\phi_e)\ . \end{aligned} \tag{10}$$

Using Eqs. (8) and (10) to carry out integration of Eq. (9), the Melnikov integral can be rewritten as

$$\begin{aligned} M(\tau_0) &= \int_{-\infty}^{+\infty} y_h(-2\mu y_h + f_m + \Omega_e^2 f_e \cos(\Omega_e(\tau+\tau_0)+\phi_e))d\tau \\ \Rightarrow M(\tau_0) &= \int_{-\infty}^{+\infty} \left(\mp\sqrt{\frac{2}{c}}a \times \operatorname{sech}(\sqrt{a}\tau)\tanh(\sqrt{a}\tau)\right)\left(-2\mu(\mp\sqrt{\frac{2}{c}}a \times \operatorname{sech}(\sqrt{a}\tau)\tanh(\sqrt{a}\tau)) + f_m + f_e\Omega_e^2\cos(\Omega_e(\tau+\tau_0)+\phi_e)\right)d\tau \end{aligned} \tag{11}$$

After evaluation of the above integral, the Melnikov function is given by

$$M^{\pm}(\tau_0) = -\frac{8}{3}\frac{\mu(a)^2}{c\sqrt{a}} \ \pm\ \sqrt{\frac{2}{c}}f_e\Omega_e^3\pi \ \times\ \operatorname{sech}\left(\frac{\pi\Omega_e}{2\sqrt{a}}\right)\sin(\Omega_e\tau_0+\phi_e)\ . \tag{12}$$

Using this equation, the condition for transverse intersection of the stable and unstable manifolds is obtained as

$$\left|-\frac{8}{3}\frac{\mu(a)^2}{c\sqrt{a}}\right| < \left|\sqrt{\frac{2}{c}}f_e\Omega_e^3\pi \ \times\ \operatorname{sech}\left(\frac{\pi\Omega_e}{2\sqrt{a}}\right).\right| \tag{13}$$

From this relation, the threshold values for the occurrence of homoclinic bifurcation and transition to chaotic behavior are obtained.

4. Controller design based on chaos control concept

This section presents the design of a practical control model for a gear system for which homoclinic bifurcation and consequently chaotic behavior can be eliminated. To this end, a non-feedback control approach is used to control chaos by applying an additional excitation torque to the driver gear. For the practical implementation of this concept, the gear body and corresponding shaft are

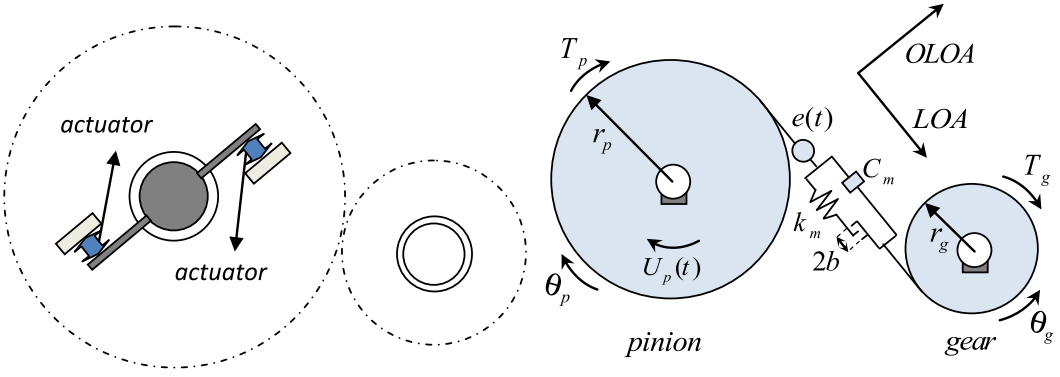

Fig. 3. Schematic of the controlled gear model including the actuator.

connected via several actuators for one set of gear–shaft coupling, as shown in Fig. 3. These actuators can transmit the mean torque and simultaneously generate additional excitation torque. The suitable parameter spaces for the additional excitation, where homoclinic chaos can be eliminated, are obtained analytically by generalization of Melnikov approach. The dynamic equations of this system including the actuator can be rewritten as

$$I_p\frac{d^2\theta_p}{dt^2}+r_pc_m\left(r_p\frac{d\theta_p}{dt}-r_g\frac{d\theta_g}{dt}-\frac{de}{dt}\right)+r_pk_mf_h\left(r_p\theta_p-r_g\theta_g-e(t)\right)=T_p+U_p(t) \tag{14-a}$$

$$I_g\frac{d^2\theta_g}{dt^2}-r_gc_m\left(r_p\frac{d\theta_p}{dt}-r_g\frac{d\theta_g}{dt}-\frac{de}{dt}\right)-r_gk_mf_h\left(r_p\theta_p-r_g\theta_g-e(t)\right)=-T_g. \tag{14-b}$$

The additional external excitation $U_p(t)$ is the chaos elimination excitation and is considered as harmonic with $U_p(t)=U_p\cos(\omega_pt+\phi_p)$. Where U_p, ω_p, and ϕ_p are the amplitude, frequency, and phase of the excitation term, respectively. Similar to Eq. (1-a to 1-b), the vibration Eq. (14-a to 14-b) can be simplified as

$$m\frac{d^2\tilde{x}}{dt^2}+c_m\frac{d\tilde{x}}{dt}+k_mf_h(\tilde{x})=\hat{F}_m+\hat{F}_e(t)+\hat{F}_p\cos\left(\omega_pt+\phi_p\right)\ . \tag{15}$$

Where $\hat{F}_p=mr_pU_p/I_p$. Further, by defining the dimensionless excitation frequency and amplitude as $\Omega_p=\omega_p/\omega_n$, $\tilde{F}_p=\hat{F}_p/bk_m$ and also considering the dimensionless parameters defined in Eq. (4), the following equation is obtained

$$\frac{d^2x}{d\tau^2}+2\tilde{\mu}\frac{dx}{d\tau}+f_h(x)=\tilde{F}_m+\tilde{F}_e\Omega_e^2\cos(\Omega_e\tau+\phi_e)+\tilde{F}_p\cos\left(\Omega_p\tau+\phi_p\right)\ . \tag{16}$$

The amplitude of excitation term is considered as weak perturbations as $\tilde{F}_p=\varepsilon f_p$. Similar to Eq. (6), the Melnikov function is obtained as

$$\begin{aligned}M(\tau_0)&=\int_{-\infty}^{+\infty}y_h(-2\mu y_h+f_m+\Omega_e^2f_e\cos(\Omega_e(\tau+\tau_0)+\phi_e)+f_p\cos(\Omega_p(\tau+\tau_0)+\phi_p))d\tau\\ \Rightarrow M(\tau_0)&=\int_{-\infty}^{+\infty}\left(\mp\sqrt{\frac{2}{c}}a\times\operatorname{sech}(\sqrt{a}\tau)\tanh(\sqrt{a}\tau)\right)(-2\mu\left(\mp\sqrt{\frac{2}{c}}a\times\operatorname{sech}(\sqrt{a}\tau)\tanh(\sqrt{a}\tau)\right)\ldots\\ &\quad\ldots+f_m+f_e\Omega_e^2\cos(\Omega_e(\tau+\tau_0)+\phi_e)+f_p\cos(\Omega_p(\tau+\tau_0)+\phi_p))d\tau\end{aligned} \tag{17}$$

After evaluating the above integral, the Melnikov function can be presented as

$$M^{\pm}(\tau_0)=A\pm B\sin(\Omega_e\tau_0+\phi_e)\pm C\sin\left(\Omega_p\tau_0+\phi_p\right) \tag{18}$$

with

$$A=-\frac{8}{3}\frac{\mu(a)^2}{c\sqrt{a}},\quad B=\sqrt{\frac{2}{c}}f_e\Omega_e^3\pi\ \times\ \operatorname{sech}\left(\frac{\pi\Omega_e}{2\sqrt{a}}\right),\quad C=\sqrt{\frac{2}{c}}f_p\Omega_p\pi\ \times\ \operatorname{sech}\left(\frac{\pi\Omega_p}{2\sqrt{a}}\right)\ .$$

Compared with Eq. (12), the control excitation term $\pm\sqrt{\frac{2}{c}}f_p\Omega_p\pi\ \times\ \operatorname{sech}(\frac{\pi\Omega_p}{2\sqrt{a}})\sin(\Omega_p\tau_0+\phi_p)$ appears in the Melnikov function. In the following, this function will be used to establish the chaos elimination results. The objective is to choose the control parameter values of f_p, Ω_p, and ϕ_p such that the chaotic behavior in primary system be eliminated.

As mentioned in the previous section, in the absence of chaos elimination excitation, Eq. (13) provides a condition for transverse intersection of the stable and unstable manifolds, and hence occurrence of chaotic behavior. Now, the additional excitation is added on the system, such that the Melnikov function always has the same sign. In the present case, a necessary condition for $M^{\pm}(\tau_0)$ to be the same sign for all τ_0 is obtained as [15]

$$\begin{aligned}&|C|>|B|-|A|=C_{\min}\\ &\left|\sqrt{\frac{2}{c}}f_p\Omega_p\pi\ \times\ \operatorname{sech}\left(\frac{\pi\Omega_p}{2\sqrt{a}}\right)\right|>\left|\sqrt{\frac{2}{c}}f_e\Omega_e^3\pi\ \times\ \operatorname{sech}\left(\frac{\pi\Omega_e}{2\sqrt{a}}\right)\right|\ -\ \left|-\frac{8}{3}\frac{\mu(a)^2}{c\sqrt{a}}\right|\ .\end{aligned} \tag{19}$$

The optimal excitation phase ($\phi_p = \phi_{optimum}$), which corresponds to the widest amplitude range for the chaos elimination, is obtained for the situation in which the maximum (maximum for A < 0 and minimum for A > 0) of $A \pm B\sin(\Omega_e\tau_0 + \phi_e)$ and $\mp C_{\min}\sin(\Omega_p\tau_0 + \phi_{optimum})$ occur at the same τ_0. In the following, B and C will be considered to be the same sign and also as a positive term. It is clear that changing this sign is equivalent to shift the phase as $\phi_e \to \tilde{\phi}_e + \pi$. In this case, for $\Omega_p = m\Omega_e$, ($m = 1, 2, 3, \ldots$), two different sets of the optimal values of excitation phase are obtained as

$$for\left(M^{+}\,and\,A<0\right)or\left(M^{-}\,and\,A>0\right)\Rightarrow\phi_{optimum}=\begin{cases}(\pi+\phi_e) & for\ (m=4n-3)\\ \left(\pi/_2+\phi_e\right) & for\ (m=4n-2)\\ (0+\phi_e) & for\ (m=4n-1)\\ \left(3\pi/_2+\phi_e\right) & for\ (m=4n)\end{cases}$$
$$for\left(M^{+}\,and\,A>0\right)or\left(M^{-}\,and\,A<0\right)\Rightarrow\phi_{optimum}=\begin{cases}(\pi+\phi_e) & for\ (m=4n-3)\\ \left(\pi/_2+\phi_e\right) & for\ (m=4n)\\ (0+\phi_e) & for\ (m=4n-1)\\ \left(3\pi/_2+\phi_e\right) & for\ (m=4n-2)\end{cases}. \tag{20}$$

Moreover, for the optimal excitation phase the upper threshold value of excitation amplitude can be easily obtained, for which $M^{\pm}(\tau_0)$ have the same sign for all τ_0. Also, the Melnikov function indicated that the excitation phase can be changed in allowed interval as $[\phi_{optimum} - \Delta\phi_{\max}\ ,\ \phi_{optimum} + \Delta\phi_{\max}]$, such that the Melnikov function always have the same sign. $\Delta\phi_{\max}$, is the maximum deviation of excitation phase from optimal phase. It is clear that the maximum deviation of excitation phase is obtained based on the nearest zeros of $A \pm B\sin(\Omega_e\tau_0 + \phi_e)$ and $\pm C\sin(\Omega_p\tau_0 + \phi_{optimum})$ given by

$$\Delta\phi_{\max} = \Omega_p\left(\tau_0^2 - \tau_0^1\right) = m\left(\arcsin\frac{A}{B} - \phi_e\right) - k\pi + \phi_{optimum}\ . \tag{21}$$

The value of τ_0^1 and τ_0^2 is the nearest zeros of $\pm C\sin(\Omega_p\tau_0 + \phi_{optimum})$ and $A \pm B\sin(\Omega_e\tau_0 + \phi_e)$, respectively. For an arbitrary deviation of excitation phase from $\phi_{optimum}$ ($0 < \Delta\phi < \Delta\phi_{\max}$), one can easily obtain the allowed amplitude value of C_{max}($<C_{max}$ at $\phi_{optimum}$), and C_{min}($>C_{min}$ at $\phi_{optimum}$). Therefore, there exist certain suitable excitation phase and amplitude intervals for controlling the chaotic behavior in a gear system.

5. Simulation results and discussion

In this section, numerical simulations are presented to demonstrate the accuracy of the theoretical predictions, and also to investigate the performance of the proposed control system to eliminate the homoclinic bifurcation and chaos in nonlinear gear systems. As mentioned in Section 3, in the absence of chaos elimination excitation, Eq. (13) provides the conditions for which the Melnikov function changes its sign (to have simple zeros). Fig. 4(a) shows the Melnikov threshold surface for the occurrence of homoclinic bifurcation in the parameter space (μ, f_e, Ω_e). In the parameter region below the threshold surface, both $M^{+}(\tau_0)$ and $M^{-}(\tau_0)$ change their sign. As a result, in this region transverse intersection of the stable and unstable manifolds occurs, appearance of chaos is expected.

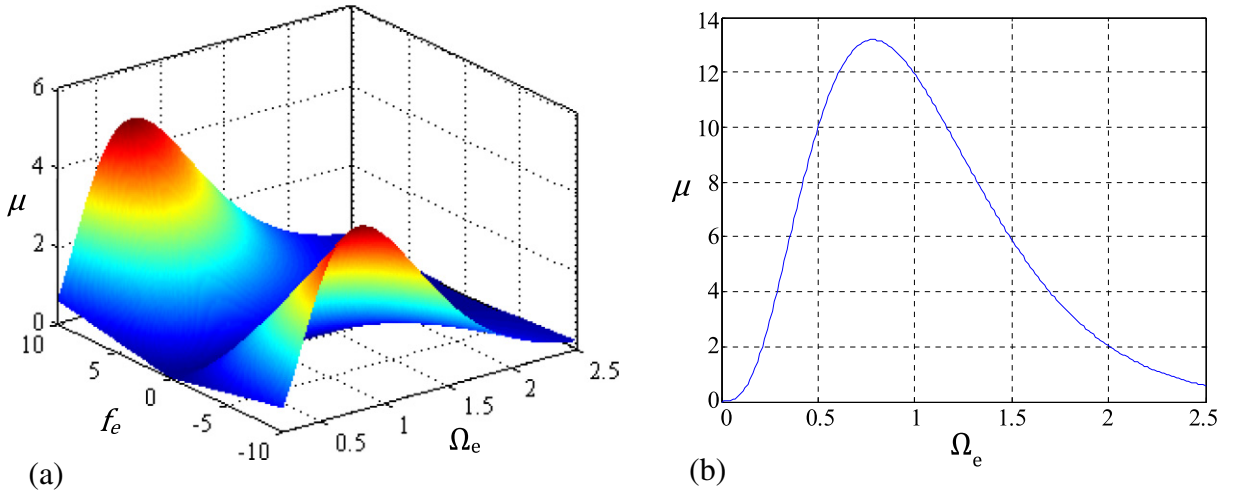

Fig. 4. (a) Threshold surface in the parameter space (μ, f_e, Ω_e), (b) threshold curve in the (μ, Ω_e) plane for $f_e = 28$.

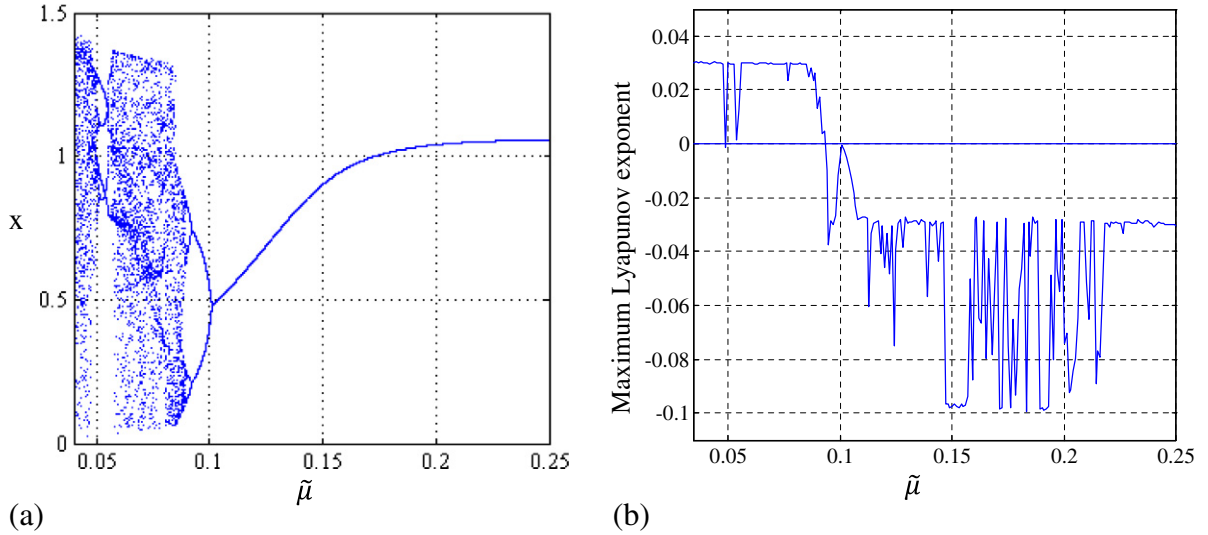

Fig. 5. (a) Bifurcation diagram, and (b) corresponding maximum Lyapunov exponent for $\tilde{\mu}$ ($\tilde{\mu} = \varepsilon\mu$) as the control parameter.

According to Eq. (13) and by choosing μ as the control parameter, the condition for transverse intersection of the stable and unstable manifolds is obtained as

$$\mu < \frac{3}{4a}\sqrt{\frac{c}{2a}}|f_e|\pi\Omega_e^3 \quad \times \quad \mathrm{sech}\left(\frac{\pi\Omega_e}{2\sqrt{a}}\right),\ for\,(\mu > 0) \quad . \tag{22}$$

The critical values of μ versus frequency Ω_e, at $f_e = 28$ are plotted in Fig. 4(b). In the region below the threshold curve the system has transverse homoclinic orbits and resulting occurrence of the chaotic behavior.

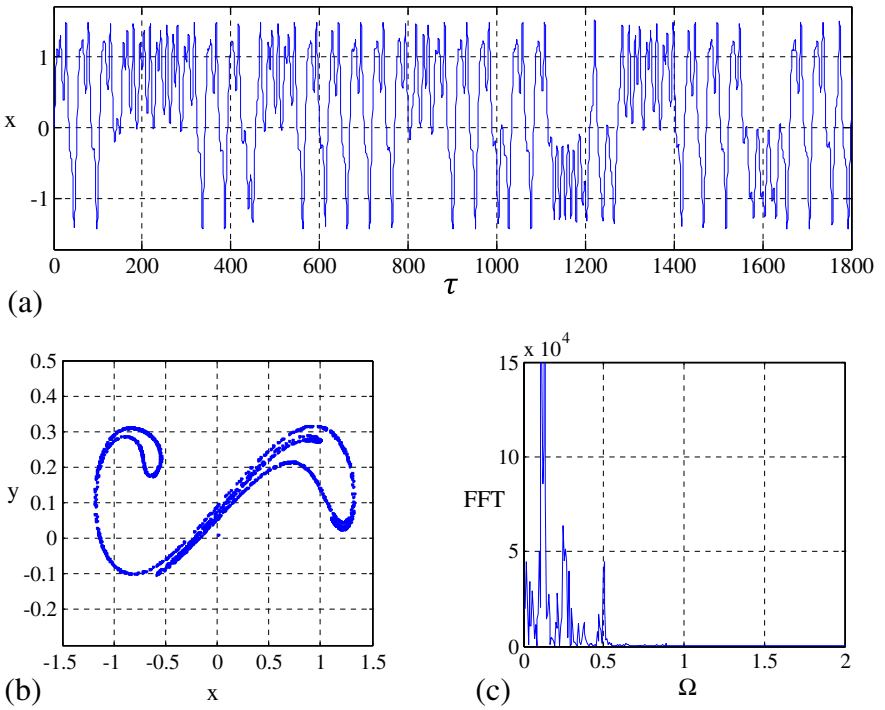

Fig. 6. (a) Time history, (b) Poincare section, and (c) Fourier spectra for μ = 8.

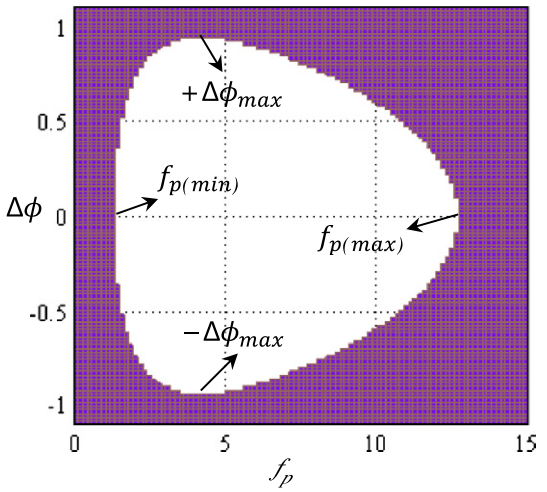

Fig. 7. The suitable amplitude and phase intervals for chaos elimination excitation.

In order to verify the analytical predictions, the bifurcation and maximum Lyapunov exponent diagrams are exhibited corresponding to some control parameters. Fig. 5(a) presents the bifurcation diagram of the system Eq. (5) for control parameter $\tilde{\mu}$ ($\tilde{\mu} = \varepsilon\mu$) at $f_m = 1$, $\Omega_e = 0.5$, $f_e = 28$, $\varepsilon = 0.01$ and initial conditions $x = 0.01$ and $\dot{x} = 0.01$. Periodic and chaotic behaviors are clearly visible at some values of control parameter, when $\tilde{\mu}$ is increased from 0 to 0.25. Observe that the gear system exhibits the period doubling bifurcation and also transition to the chaotic responses at low values of $\tilde{\mu}$, i.e., $\tilde{\mu} < 0.101$. The corresponding maximum Lyapunov exponent diagram is also plotted in Fig. 5(b). The positive Lyapunov exponents are characteristic of chaotic behaviors. As expected, one can see a good agreement between the bifurcation diagrams and the maximum Lyapunov exponent diagram. According to Fig. 4(b), in $\Omega_e = 0.5$, the theoretical prediction for the occurrence of homoclinic bifurcation is obtained at $\mu \cong 10.06$, which is in good agreement with the numerical simulation results.

Now the system parameters are chosen as $f_e = 28$, $\Omega_e = 0.5$, $f_m = 1$, and $\mu = 8$, and controlling of chaotic behavior for this case is considered. According to Fig. 4, it can be observed that this point situates below the threshold value and corresponds to the

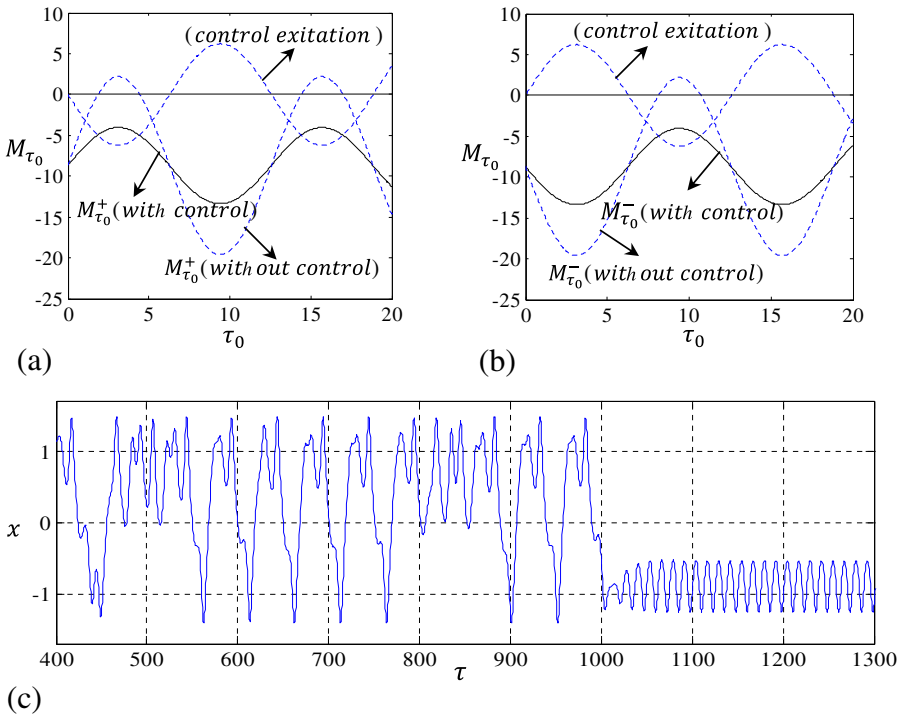

Fig. 8. Uncontrolled and controlled systems at $f_p = 4$, $\phi_p = \pi$, (a) $M^+_{\tau_0}$, (b) $M^-_{\tau_0}$, and (c) time response.

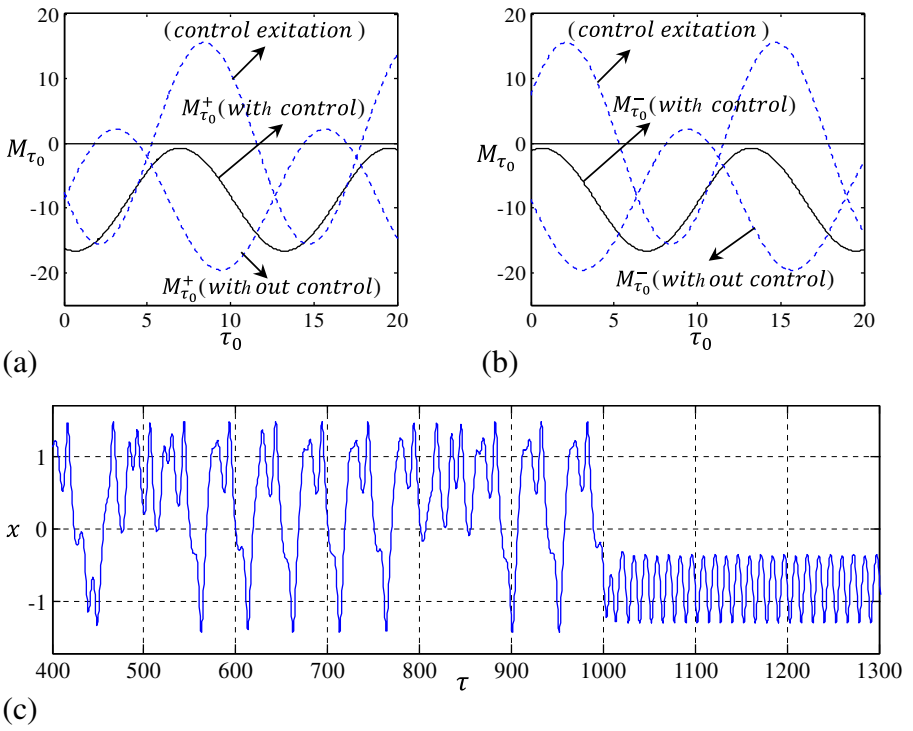

Fig. 9. Uncontrolled and controlled systems at $f_p = 10$, $\phi_p = \pi + 0.5$, (a) $M^{+}_{\tau_0}$, (b) $M^{-}_{\tau_0}$, and (c) time response.

chaotic motion (see Fig. 5). The numerical simulation of Eq. (5) is performed for this point. The chaotic motion is identified from the time history, Poincare section and Fourier spectra, as shown in Fig. 6.

Now, the additional excitation $U_p(t)$ is added on the chaotic system. When $U_p(t)$ affects the system, the control excitation term $\pm\sqrt{\frac{2}{c}} f_p \Omega_p \pi \times \mathrm{sech}(\frac{\pi\Omega_p}{2\sqrt{a}}) \sin(\Omega_p \tau_0 + \phi_p)$, appears in the Melnikov function. The objective is to choose the control parameter values of f_p, Ω_p, and ϕ_p, such that the chaotic behavior in primary system be eliminated. The frequency of the excitation term is chosen as $\omega_p = \omega_e$ in the following. According to Eq. (20), the optimal value of excitation phase is $\phi_{optimum} = \pi + \phi_e$. Thus, for this optimal phase the lower and upper threshold values of excitation amplitude are obtained as

$$C_{\min} = |B| - |A| = \sqrt{\frac{2}{c}} f_{p(\min)} \Omega_p \pi \times \mathrm{sech}\left(\frac{\pi\Omega_p}{2\sqrt{a}}\right) = 2.1842 \Rightarrow f_{p(\min)} = 1.4$$

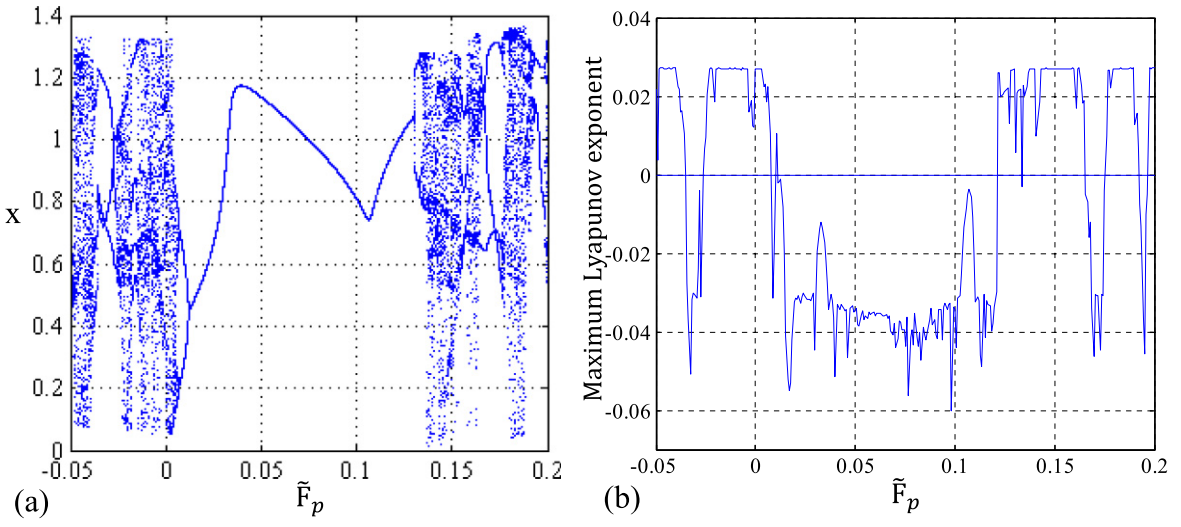

Fig. 10. (a) Bifurcation diagram, and (b) corresponding maximum Lyapunov exponent diagram for control parameter $\tilde{F}_p$ at $\phi_p = \pi$.

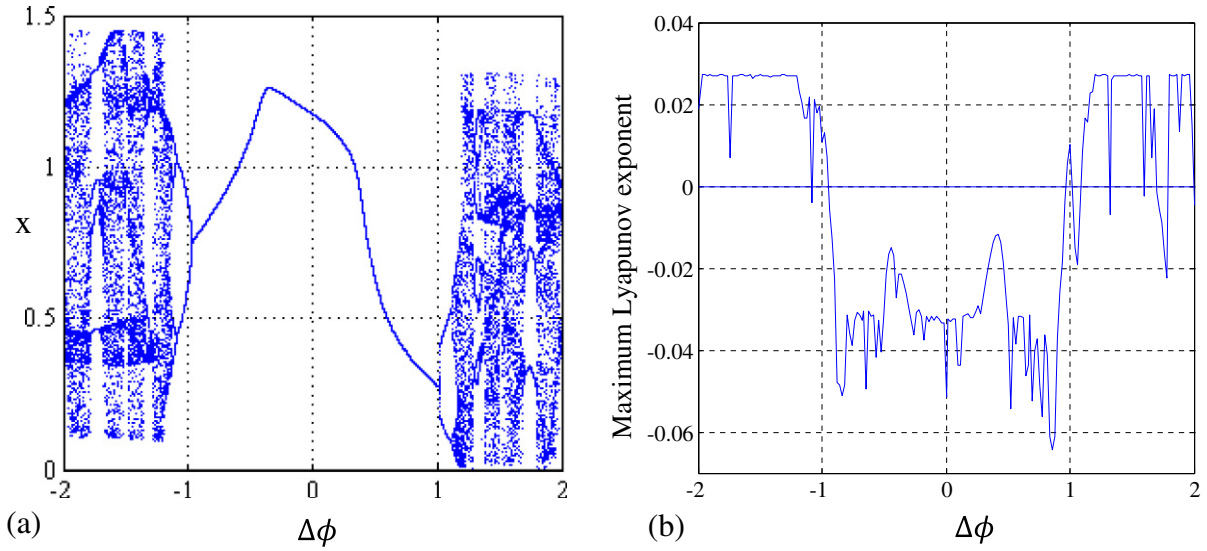

Fig. 11. (a) Bifurcation diagram, and (b) corresponding maximum Lyapunov exponent diagram for control parameter $\Delta\phi$ at $f_p = 4$.

and

$$C_{\max} = |B| + |A| = \sqrt{\frac{2}{c}} f_{p(\max)} \Omega_p \pi \times \operatorname{sech}\left(\frac{\pi\Omega_p}{2\sqrt{a}}\right) = 19.6046 \Rightarrow f_{p(\max)} = 12.6 \ .$$

Thus, for $\phi_{optimum} = \pi + \phi_e$, the maximum theoretical interval of excitation amplitude is approximately $f_p = [1.4 \ \ 12.6]$. By using Eq. (21), the maximum deviation of excitation phase from $\phi_{optimum}$ is obtained as

$$\Delta\phi_{\max} = \Omega_p\left(\tau_0^2 - \tau_0^1\right) = \arcsin\frac{A}{B} = 0.926 \ .$$

The maximum allowed interval of excitation phase is now $\phi_p = [\pi + \phi_e - 0.926 \ \ \pi + \phi_e + 0.926 \ ]$. For each value of ϕ_p belonging to such interval there is certain suitable amplitude. The suitable amplitude and phase intervals for the control excitation

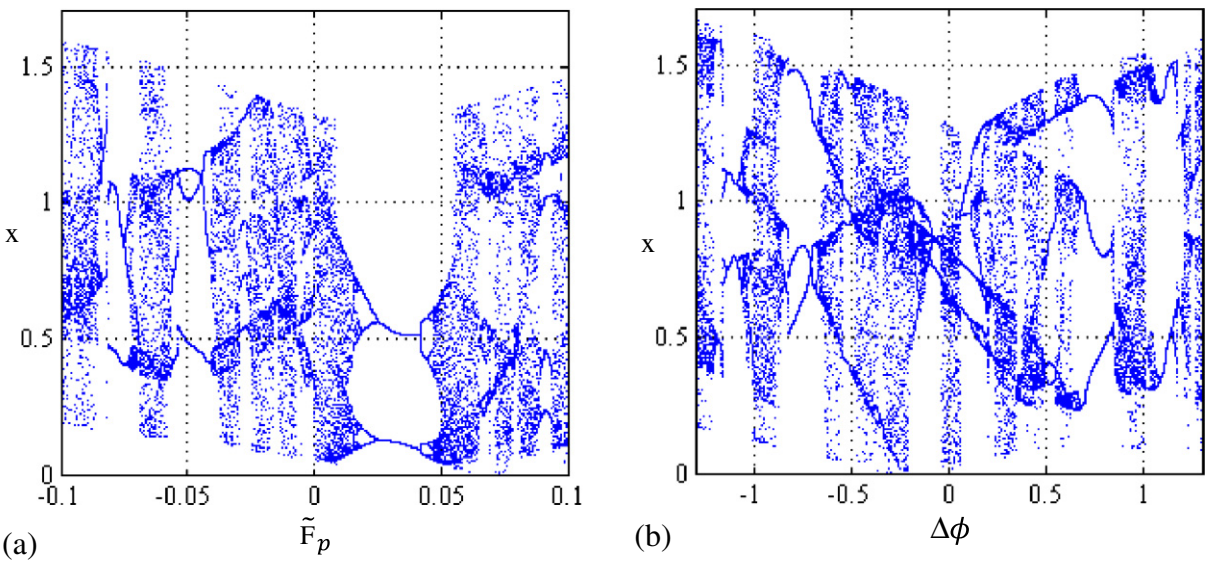

Fig. 12. Bifurcation diagram for: (a) control parameter $\tilde{F}_p$ at $\phi_p = \pi + 1.1$, (b) control parameter $\Delta\phi$ at $f_p = 14$.

term are shown in Fig. 7 (white region). By selecting the additional excitation belonging to this interval, chaotic motion can be controlled. To illustrate the accuracy of the analytical predictions, the time responses and the Melnikov function for the parameters $\phi_e = 0$, $\Omega_p = 0.5$ and two values of f_p and ϕ_p, are shown in Figs. 8 and 9. Fig. 8(a) and (b) shows the Melnikov function associated with the values $f_p = 4$, and $\phi_p = \pi$. After the additional excitation is added on the system, Melnikov functions do not change their sign, for which elimination of chaotic behavior is expected. The time history of this point is given in Fig. 8(c). According to this figure, as controller is implemented at $\tau = 1000$, chaotic motion is vanished and lead to the appearance of periodic response. Also, Fig. 9 demonstrates controlling the chaos for the control excitation parameters $f_p = 10$, $\phi_p = \pi + 0.5$. Observe that after the additional excitation is added on the system, the Melnikov functions do not change sign (Fig. 9(a) and (b)), and thus elimination of chaos is occurred (Fig. 9(c)).

In the following, the dynamic behaviors of system are shown using bifurcation and maximum Lyapunov exponent diagrams for some system parameters. The theoretical intervals are compared with the numerical intervals of chaos elimination obtained using the bifurcation diagrams and the maximum Lyapunov exponent diagrams. According to Fig. 7, when the value of ϕ_p is $\phi_{optimum}$, the allowed amplitude interval is $\tilde{F}_p = [0.014\ 0.126]$, and hence corresponds to the widest amplitude interval for the chaos elimination excitation. Fig. 10(a) presents the bifurcation diagram for control parameter $\tilde{F}_p = \varepsilon f_p$ at $\Omega_e = \Omega_p = 0.5$, $f_m = 1$, $\mu = 8$, $f_e = 28$, $\varepsilon = 0.01$ and $\phi_p = \pi$. Fig. 10(b) presents the corresponding maximum Lyapunov exponent diagram for these values of the parameters. From these figures, the numerical interval of chaos elimination is [0.013 0.13] and confirms the theoretical prediction. The bifurcation diagram and the corresponding maximum Lyapunov exponent for control parameter $\Delta\phi$ at $f_p = 4$, are shown in Fig. 11. The theoretical interval of $\Delta\phi$ is now $[-0.926\ 0.926]$, and the numerical results show the chaos elimination interval as $[-0.96\ 1.01]$. Fig. 12(a) and (b) shows the bifurcation diagrams for control parameter $\tilde{F}_p = \varepsilon f_p$ at $\phi_p = \pi + 1.1$ and for control parameter $\Delta\phi$ at $f_p = 14$, which are not in the suitable interval, chaos elimination is not expected. The numerical simulations confirm the theoretical predictions and show the efficiency of the proposed system to control the homoclinic bifurcation and consequently chaos elimination in a gear system.

6. Conclusion

In this paper, a practical model of gear system has been proposed to control and eliminate the chaotic behaviors. To this end, non-feedback control method has been used to control the chaos by applying an additional excitation torque to the driver gear. The parameter spaces of the control excitation, where homoclinic chaos can be eliminated, have been obtained analytically by generalization of Melnikov approach. The controller performance has been validated with the numerical simulations. Numerical simulation results show effectiveness of the proposed system to control the homoclinic bifurcation and chaos in gear system. The proposed control system can be easily realized in practical system and can be used for design and development of an optimal gear transmission system.

References

[1] A. Kahraman, G.W. Blankenship, Experiments on nonlinear dynamic behavior of an oscillator with clearance and periodically time-varying parameters, J. Appl. Mech. 64 (1997) 217–226.
[2] G.W. Blankenship, A. Kahraman, A steady state forced response of a mechanical oscillator with combined parametric excitation and clearance type non-linearity, J. Sound Vib. 185 (5) (1995) 743–765.
[3] A. Raghothama, S. Narayanan, Bifurcation and chaos in geared rotor bearing system by incremental harmonic balance method, J. Sound Vib. 226 (3) (1999) 469–475.
[4] J. Wang, T.C. Lim, M. Li, Dynamics of a hypoid gear pair considering the effects of time-varying mesh parameters and backlash nonlinearity, J. Sound Vib. 308 (2007) 302–329.
[5] J. Luczko, Chaotic vibrations in gear mesh systems, J. Theor. Appl. Mech. 46 (4) (2008) 879–896.
[6] J. Wang, J. Zheng, A. Yang, An analytical study of bifurcation and chaos in a spur gear pair with sliding friction, Proc. Eng. 31 (2012) 563–570.
[7] C.W. Chang-Jian, Sh.M. Chang, Bifurcation and chaos analysis of spur gear pair with and without nonlinear suspension, Nonlinear Anal. Real World Appl. 12 (2011) 979–989.
[8] C.W. Chang-Jian, Strong nonlinearity analysis for gear-bearing system under nonlinear suspension bifurcation and chaos, Nonlinear Anal. Real World Appl. 11 (2010) 1760–1774.
[9] C.C. Hwang, J.Y. Hsieh, R.S. Lin, A linear continuous feedback control of Chua's circuit, Chaos, Solitons Fractals 8 (9) (1997) 1507–1515.
[10] F.N. Koumboulis, B.G. Mertzios, Feedback controlling against chaos, Chaos, Solitons Fractals 11 (2000) 351–358.
[11] A. Hegazi, H.N. Agiza, M.M.E. Dessoly, Controlling chaotic behavior for spin generator and Rossler dynamical systems with feedback control, Chaos, Solitons Fractals 12 (2001) 631–658.
[12] H.N. Agiza, Controlling chaos for the dynamical system of coupled dynamics, Chaos, Solitons Fractals 13 (2002) 341–352.
[13] A. Uchida, S. Kinugawa, S. Yoshimori, Synchronization of chaos in two microship lasers by using incoherent feedback method, Chaos, Solitons Fractals 17 (2003) 363–368.
[14] F.M. Moukam Kakmeni, S. Bowong, C. Tchawoua, E. Kaptouom, Resonance, bifurcation and chaos control in electrostatic transducers with two external periodic forces, Physica A 333 (2004) 87–105.
[15] R. Chacon, General results on chaos suppression for biharmonically driven dissipative systems, Phys. Lett. A 257 (1999) 293–300.
[16] M. Belhaq, M. Houssni, Suppression of chaos in averaged oscillator driven by external and parametric excitations, Chaos, Solitons Fractals 11 (2000) 1237–1246.
[17] R. Chacon, Role of ultra subharmonic resonances in taming chaos by weak harmonic perturbations, Europhys. Lett. 54 (2) (2001) 148–153.
[18] R. Wang, J. Deng, Z. Jing, Chaos control in duffing system, Chaos, Solitons Fractals 27 (2006) 249–257.
[19] X. Wu, J. Lu, Iu H. Ho-Ching, S.Ch. Wong, Suppression and generation of chaos for a three-dimensional autonomous system using parametric perturbations, Chaos, Solitons Fractals 31 (2007) 811–819.
[20] J. Yang, Z. Jing, Controlling chaos in a pendulum equation with ultra-subharmonic resonances, Chaos, Solitons Fractals 42 (2009) 1214–1226.
[21] R. Chacon, A.M. Lacasta, Controlling chaotic transport in two-dimensional periodic potentials, Phys. Rev. E 82 (2010) 046207.
[22] E. Ott, N. Grebogi, J. Yorke, Controlling chaos, Phys. Rev. Lett. 64 (11) (1990) 1196–1199.

[23] Y. Shen, S. Yang, X. Liu, Nonlinear dynamics of a spur gear pair with time-varying stiffness and backlash based on incremental harmonic balance method, Int. J. Mech. Sci. 48 (2006) 1256–1263.
[24] G. Bonori, F. Pellicano, Non-smooth dynamics of spur gears with manufacturing errors, J. Sound Vib. 306 (2007) 271–283.
[25] A. Farshidianfar, A. Saghafi, Global bifurcation and chaos analysis in nonlinear vibration of spur gear systems, Nonlinear Dyn. 75 (2014) 783–806.
[26] S. Wiggins, Global Bifurcations and Chaos, Springer, New York, 1988.
[27] S. Wiggins, Introduction to Applied Nonlinear Dynamical Systems and Chaos, Springer, NewYork, 1990.
[28] M. SieweSiewe, F.M. MoukamKakmeni, C. Tchawoua, P. Woafo, Bifurcations and chaos in the triple-well φ^6 Van der Pol oscillator driven by external and parametric excitations, Physica A 357 (2005) 383–396.
[29] J. Awrejcewicz, Y. Pyryev, Chaos prediction in the duffing-type system with friction using Melnikov's function, Nonlinear Anal. RealWorld Appl. 7 (2006) 12–24.
[30] K. Yagasaki, Bifurcations and chaos in vibrating micro cantilevers of tapping mode atomic force microscopy, Int. J. Non-Linear Mech. 42 (2007) 658–672.
[31] M. SieweSiewe, H. Cao, M. Sanjuan, On the occurrence of chaos in a parametrically driven extended Rayleigh oscillator with three-well potential, Chaos, Solitons Fractals 41 (2009) 772–782.
[32] G. Litak, M. Borowiec, A. Syta, K. Szabelski, Transition to chaos in the self-excited system with a cubic double well potential and parametric forcing, Chaos, Solitons Fractals 40 (2009) 2414–2429.
[33] L. Zhou, Y. Chen, F. Chen, Global bifurcation analysis and chaos of an arch structure with parametric and forced excitation, Mech. Res. Commun. 37 (1) (2010) 67–71.